EFFECTS OF INLET SWIRL ON THE PERFORMANCE OF ANNULAR JET PUMP

Tohru Maeda
Graduate School of Mechanical Engineering, Science University of Tokyo
Kagurazaka, Shinjuku-ku, Tokyo, 162-8601, Japan

Osamu Kitamura and Makoto Yamamoto
Department of Mechanical Engineering, Science University of Tokyo
Kagurazaka, Shinjuku-ku, Tokyo, 162-8601, Japan

ABSTRACT

Jet pumps have been used in a lot of engineering fields. However, since the efficiency is generally low, it has been needed to improve the performance. We have numerically studied an annular jet pump without inlet swirl, and confirmed that a Reynolds stress model can reasonably predict the flow field, and the inlet swirl has the possibility to control the performance. In the present study, annular jet pumps with inlet swirl are calculated with a standard Reynolds stress turbulence model, to clarify the effects of inlet swirl of the driving jet on the mean flow field and the performance. It is shown that the inlet swirl does not change the mean flow fields remarkably, but suitable inlet swirl can contribute to the improvement of the efficiency. Moreover, it is indicated that the standard Reynolds stress model is insensitive to the change of inlet swirl.

INTRODUCTION

Jet pumps have been used in a great number of engineering applications because of the simple construction and easy operation. Many theoretical, experimental and/or numerical investigations have been reported in literatures. It is well known that the efficiency of a jet pump is generally low, because the driving principle is based on turbulent mixing between the high-speed jet and the low-speed suction fluid. However, since the previous studies focused on only the efficiency, the turbulent flow field within a jet pump has not been understood satisfactorily. Therefore, the design is mainly dependent on experimental correlations or empiricism even now.

Jet pumps are commonly classified into three types by the geometry (i.e. central, annular and bend types). We have been investigating an annular jet pump. Fig.1 shows the schematic of an annular jet pump. This pump uses a high-speed jet to entrain a low-speed flow from the central pipe. An annular jet pump has been experimentally studied by some researchers such as Shimizu et al. (1985, 1987) and Elger et al.(1991, 1994). In our previous study (Namiki et al., 1997), we calculated the flow field in the annular jet pump measured by Shimizu et al. (1985, 1987). From the computations, it was shown that a large recirculation in the mixing chamber (i.e. the convergent nozzle and throat parts) is formed at relatively low Reynolds number. And it was also confirmed that a standard k- ε model always underestimates the head ratio and the efficiency because of the overestimation of turbulent mixing, whereas a standard Reynolds stress model can satisfactorily predict them (see Fig.2). In addition, it was clarified that to keep the lower static pressure within the mixing chamber is preferable to its efficiency, and the inlet swirl could have a possibility to make a significant contribution to the extension of the operating range of an annular jet pump.

In the present study, we numerically investigate the effects of the inlet swirl of the driving jet on the mean flow field and the performance. Employing the standard Reynolds stress model developed by Gibson and Launder (1978), the flow fields under different conditions of inlet swirl and Reynolds number are simulated. Based on the computational results, the mean flow properties and turbulent quantities are investigated. Moreover, it is discussed how turbulence and inlet swirl contribute to the performance of the annular jet pump.

NUMERICAL PROCEDURES

The flow field was assumed to be incompressible, steady, axisymmetric and fully turbulent. Therefore, we adopted Reynolds-averaged Navier-Stokes equations with incorporating the standard Reynolds stress turbulence model proposed by Gibson and Launder (1978). The model equations for Reynolds stresses and dissipation rate of turbulent kinetic energy can be expressed as follows.

$$\frac{D\overline{u_i u_j}}{Dt} = D_{ij} + P_{ij} + \Phi_{ij} - \frac{2}{3}\varepsilon\delta_{ij} \tag{1}$$

$$\frac{D\varepsilon}{Dt} = D_{\varepsilon} + C_{\varepsilon 1}\frac{\varepsilon}{k}P_k - C_{\varepsilon 2}\frac{\varepsilon^2}{k} \tag{2}$$

$$D_{ij} = \frac{\partial}{\partial x_m}\left(C_s\overline{u_i u_m}\frac{k}{\varepsilon}\frac{\partial\overline{u_i u_j}}{\partial x_l}\right) \tag{3}$$

$$D_{\varepsilon} = \frac{\partial}{\partial x_m}\left(C_{\varepsilon}\overline{u_i u_m}\frac{k}{\varepsilon}\frac{\partial\varepsilon}{\partial x_l}\right) \tag{4}$$

$$P_{ij} = -\overline{u_i u_l}\frac{\partial U_j}{\partial x_l} - \overline{u_j u_l}\frac{\partial U_i}{\partial x_l} \tag{5}$$

$$\Phi_{ij} = \Phi_{ij(1)} + \Phi_{ij(2)} + \Phi^{w}_{ij(1)} + \Phi^{w}_{ij(2)} \tag{6}$$

$$\Phi_{ij(1)} = -C_1\frac{\varepsilon}{k}\left(\overline{u_i u_j} - \frac{2}{3}k\delta_{ij}\right) \tag{7}$$

$$\Phi_{ij(2)} = -C_2\left(P_{ij} - \frac{2}{3}P_k\delta_{ij}\right) \tag{8}$$

$$\Phi^w_{ij(1)} = C_1'\frac{\varepsilon}{k}\left(\overline{u_k u_m}n_k n_m\delta_{ij} - \frac{3}{2}\overline{u_i u_k}n_k n_j - \frac{3}{2}\overline{u_j u_k}n_k n_i\right)f_w \tag{9}$$

$$\Phi^w_{ij(2)} = C_2'\left(\Phi_{lm(2)}n_l n_m\delta_{ij} - \frac{3}{2}\Phi_{il(2)}n_l n_j - \frac{3}{2}\Phi_{jl(2)}n_l n_i\right)f_w \tag{10}$$

$$f_w = \frac{k^{3/2}}{C_l \varepsilon x_n} \tag{11}$$

$$C_1 = 1.8, C_2 = 0.6, C_1' = 0.5, C_2' = 0.3, C_s = 0.22, \quad C_\varepsilon = 0.18, C_{\varepsilon 1} = 1.44, C_{\varepsilon 2} = 1.92, C_l = 2.5 \tag{12}$$

These governing equations expressed on Cartesian coordinates (x, y, z) were transformed into those on cylindrical coordinates (x, r, θ). And then, remaining the dependent variables on cylindrical coordinates, they were transformed into those on generalized coordinates (ξ, η, ζ) to express the boundaries exactly. The equations finally obtained were discretized by finite difference schemes. A 3rd order upwind scheme proposed by Kawamura and Kuwahara (1985) was employed for the convective terms appearing in each equation, and a 2nd order central differencing scheme for other terms. All variables were assigned on a same grid point (i.e. a regular grid system). MAC method was used to obtain the converged solutions for these governing equations as the asymptotic state.

We calculated two types of annular jet pumps. The convergence angle of the nozzle and the width of the driving high-speed jet are different each other. Two pumps are referred to Type-1 and Type-2, respectively. Table 1 lists the dimensions of these pumps. It is experimentally reported that Type-1 has relatively high efficiency, and Type-2 has large mass flow rate.

Fig.3 shows the computational domain, the coordinate system, and the velocity components used in the present study. The nozzle and throat parts (shaded in the figure) are very important because the performance of an annular jet pump strongly depends on the configuration. In other words, the flow pattern within this region determines the efficiency. And these parts are called as "Mixing Chamber".

All computations were performed using 148×80 grid points in axial and radial directions, respectively. A lot of grid points were clustered near the jet exit and the walls to resolve the steep gradients of flow variables. Grid independence of the solutions was checked, using 148×56, 148×68, and 148×80 grid systems at Reynolds number of 6.6×10^5. It was found that the efficiency approaches an asymptotic value, and the deviation between 148×68 and 148×80 grid systems was only 0.4%. Taking into account this result and our computer hardware (Alpha, 433Hz), we decided to use the grid system of 148×80 in all calculations.

To obtain the performance curves of the annular jet pump, computations were carried out at 3 Reynolds numbers (5.5, 6.6 and 7.7×10^5). The ratio (V_ϕ) of the circumferential velocity to the axial one of the driving jet was changed from 0.04 to 0.29 to make the effect clear.

In the present study, boundary conditions were imposed as follows.

Inlet boundary of the driving jet ("BJ" in Fig.3): After calculating a fully developed turbulent flow in a coaxial pipe, the solutions were fixed as this boundary condition. In the cases with inlet swirl, the swirl velocity was assumed to be a 1/7 power law with the maximum velocity and the boundary layer thickness of half- height of the driving jet, since the information was not reported in the experiment.

Inlet boundary of the secondary flow ("BS" in Fig.3): The mean velocity profile was extrapolated from the inner region. And the mean static pressure was given, assuming next Bernoulli's law,

$$P_{atm} = \frac{1}{2}\rho U_s^2 + P_s + \rho g H_s \tag{13}$$

where subscript "s" denotes the inlet of the suction pipe and all physical quantities are averaged over the cross section. Atmospheric pressure Patm and suction head Hs were fixed in all computations so as to match the experimental condition.

Exit boundary ("BE" in Fig.3): Similar to the inlet of the secondary flow, the velocity profile was extrapolated from the inner region, and the static pressure was calculated by applying following Bernoulli's law,

$$P_d = P_{atm} + \rho g H_d \tag{14}$$

where head Hd was fixed again, using the measurement.

Wall boundaries: A generally used wall function was adopted along each streamline, since a high-Reynolds-number type turbulence model was employed in this study. It should be noted that the shear components of Reynolds stresses were experientially fixed to be 0 on the wall to suppress numerical oscillations.

In order to estimate the performance of the jet pump, mass flow ratio M, head ratio N, efficiency η, and mean static pressure coefficient Cp were calculated, using the converged solutions for the flow fields. These parameters can be given by following equations.

$$M = \frac{Q_s}{Q_j} \tag{15}$$

$$N = \frac{(K_K - K_P)U_d^2/2g + P_d/\rho g - U_s^2/2g - P_s/\rho g}{U_j^2/2g + P_j/\rho g - (K_K - K_P)U_d^2/2g - P_d/\rho g} \tag{16}$$

$$\eta = MN \tag{17}$$

The correction factors are defined by the next equations.

$$K_K = \frac{\rho/2\int_0^{r_w} 2\pi(U^2 + W^2)Ur\,dr}{(\rho/2)U_d^2(Q_j + Q_s)} \tag{18}$$

$$K_P = \frac{\int_0^{r_w} 2\pi Ur\left\{\rho\int_r^{r_w}(W^2/r)dr\right\}dr}{(\rho/2)U_d^2(Q_j + Q_s)} \tag{19}$$

where U is axial velocity and W circumferential velocity, r radial distance from the pump axis (see Fig.3).

In the cases with inlet swirl, swirl intensity was estimated, using a non-dimensional angular momentum flux Ij' written as follows.

$$I'_j = \frac{\rho\int_0^{r_w} 2\pi UWr^2\,dr}{\rho U_d r_w (Q_j + Q_s)} \tag{20}$$

It should be noted that the quantities with any subscript, such as Uj, Qs, Ps and so forth, denote mean values over the cross section normal to the pump axis. And these quantities were estimated, by approximating the discrete data on the grid points with a 2nd order interpolation and then integrating the distribution.

RESULTS AND DISCISSION

Type-1

First, the results obtained for Type-1 will be explained and discussed.

Fig.4 shows the velocity vectors in the x-r plane under the conditions of Reynolds numbers of 5.5 and 7.7×10^5 and the non-dimensional swirl velocity of 0.04. Only the upstream half of the mixing chamber is plotted. The Reynolds number is defined, using the maximum axial velocity of the driving jet and the inner diameter of the pipe D_0. It is apparent that the mean flow pattern is nearly same as the case without inlet swirl (Namiki et al., 1997). That is, the strong recirculation is formed at low Reynolds number (see Fig.4(a)), and the secondary flow is smoothly entrained at high Reynolds number (Fig.4(b)). The anisotropy of turbulence becomes slightly stronger in the driving jet region due to the inlet swirl (not shown here), but the effect does not change the mean flow pattern remarkably.

Fig.5 depicts the mean velocity vectors in the r-θ plane. The vectors are projected onto the x-r plane. We can see that at the lower Reynolds number the large recirculation transports the angular momentum to the core region, whereas at the high Reynolds number angular momentum is not transferred towards the axis. Therefore, the effect of inlet swirl is limited within the high-speed driving jet flow, and the influence is indirectly reflected through not the turbulence but the mean flow pattern.

Fig.6 plots the predicted efficiency under different conditions of inlet swirl. In this figure, $V\phi$ denotes non-dimensional swirl velocity, and the larger $V\phi$ corresponds to the stronger swirl intensity. We can see that the Reynolds stress model always predicts the decrease of the efficiency at high swirling conditions, especially at the large mass flow ratio. Hence, too strong inlet swirl degrades the performance of this configuration of an annular jet pump. This tendency agrees well with that of experiment (Shimizu et al., 1987).

In order to make the swirling effect much clearer, the efficiency for the swirling intensity is depicted in Figs.7 and 8. Fig.7 shows the computational results at Reynolds number of 7.7×10^5 (i.e. the highest Reynolds number case). It is obvious that the Reynolds stress model predicts the monotonic decrease of efficiency with increasing the inlet swirl. Investigating the static pressure coefficient Cp, it was found that the stronger swirl makes the static pressure within the nozzle become higher, and the high pressure would prevent the secondary flow from being entrained effectively. On the other hand, looking at Fig.8 which plots the results at the lowest Reynolds number of 5.5×10^5, it is apparent that the Reynolds stress model yields the increase of efficiency at moderate swirling intensity by about 1%, and the decrease at higher swirling one by about 1%. In the case with the appropriate swirl, the static pressure in the mixing chamber is slightly higher than that in the case without swirl. But the centrifugal force by the swirl presses the driving jet against the nozzle wall, and thus the effective area for the suction flow becomes larger. Therefore, taking into account the improvement of efficiency, we can recognize that the latter effect overcomes the former one in this case. In addition, it can be confirmed that optimum inlet swirl exists to modify the efficiency.

Fig.9 shows the change of separating streamlines for different inlet swirls at Reynolds number of 7.7×10^5. As indicated in this figure, separating streamline means the streamline passing through the outer edge of the suction pipe. In other words, this line plots the mixing process of the driving jet. Since the movement of this streamline is not remarkable, the close-up view is indicated. We can easily found that the position of the streamline reflects the monotonic decrease of efficiency. That is, the streamline moves towards the pump axis with increasing the inlet swirl, and this fact means the monotonic decrease of effective area to entrain the secondary fluid. This trend is in qualitative agreement of the insight obtained in our previous study (Namiki et al., 1997).

Type-2

Next, the numerical results for Type-2 will be exhibited and discussed. Shimizu et al.(1987) reported that this pump is sensitive to the change of inlet swirl.

Fig.10 shows the mean velocity vectors in the x-r plane at Reynolds number of 7.1×10^5. Although a small separation occurs around the inlet of the throat part due to the severe turning of the flow, it is apparent that the flow pattern is similar to that of Type-1 (Fig.4(b)). It should be noted that another results on the mean velocities show same features as those of Type-1.

Fig.11 depicts the comparison of the predicted efficiency with the corresponding measurement. The reproducibility by the standard Reynolds stress model is good around mass flow ratio of 0.2. However, at the higher mass flow ratio, the predictions indicate the monotonic increase of efficiency, whereas the experiment does the rapid decrease. This trend of efficiency is responsible for the occurrence of cavitation within the throat. Since our code cannot treat cavitation, this discrepancy is unavoidable.

Fig.12 exhibits the change of efficiency for various inlet swirls. In this case, it is clear that, at every mass flow ratio, the efficiency increases monotonically with increasing the inlet swirl. The increase exceeds about 1.5%. By checking the separating streamlines, we found that this is caused from the fact that the inlet swirl effectively works to expand the area for the secondary flow.

Fig.13 shows the comparison of the computed efficiency with the measurement at Reynolds number of 7.1×10^5. The experiment indicates that the efficiency increases by about 7% with varying the inlet swirl from Ij'=0 to 1.3, but decreases at the higher swirl intensity due to cavitation. However, our calculations do not exhibit such a large increase of efficiency. Unfortunately, the Reynolds stress model would be insensitive to the change of inlet swirl. Therefore, we will need further investigations on the predictability of a Reynolds stress model for swirling wall jets to modify the computations.

Influence of Inlet Swirl

Taking into account the computations described above, we can derive following insights on the phenomena within the

jet pump.
(1) The inlet swirl presses the driving jet against the nozzle wall. Through this process, the width of the wall jet becomes smaller, and this contributes to the extension of the effective area for the suction fluid. So this is a positive effect.
(2) However, the centrifugal force acting on the jet makes static pressure become higher. The high pressure promotes the growth of the jet. This can cancel out the effect (1). Thus, this is a negative influence.
(3) The efficiency of a jet pump may depend on the balance of these two phenomena. Therefore, it is needed to select a optimum inlet swirl to improve the performance for any configuration and working condition.

SUMMARY

In the present study, computations of the performance of an annular jet pump with inlet swirl of the driving jet were carried out, and the contributions of the mean flow, turbulence and the inlet swirl to the efficiency were discussed. Using a standard Reynolds stress model, the turbulent flow fields at a wide variety of inlet swirl intensities were calculated, and the performance parameters were predicted numerically. The computational results suggested that the suitable inlet swirl can contribute to the extension of the working area of an annular jet pump. The improvement of efficiency is dependent on the balance of two effects (i.e. the extension of effective area for secondary fluid and the static pressure rise). Moreover, it was confirmed that the Reynolds stress model is insensitive to the inlet swirl, and thus further investigations will be needed to modify the predictions.

REFERENCES

Elger,D.F., McLam,E.T. and Taylor,S.J., "A New Way to Represent Jet Pump Performance", Trans. ASME, J. Fluids Eng., 113, (1991), 439-444

Elger,D.F., Taylor,S.J. and Liou,C.P., "Recirculation in an Annular-Type Jet Pump", Trans. ASME, J. Fluids Eng., 116, (1994), 735-739

Gibson, M.M. and Launder, B.E., "Ground Effects on Pressure Fluctuations in the Atomospheric Boundary Layer", J.Fluid Mech., 86, (1978), 491-511

Kawamura,T. and Kuwahara,K., "Direct Numerical Simulation of a Turbulent Inner Flow by Finite-Difference Method", AIAA Paper 85-376, (1985), 1-10

Namiki,N., Kitamura,O. and Yamamoto,M., "Numerical Prediction of Performance of Annular Jet Pump", Proc. 11th Symp. on Turbulent Shear Flows, (1997), P2.19-24

Shimizu, Y., Nakamura,S. and Kuzuhara,S, " On Annular Jet Pumps", Turbomachinery, 13-6, (1985), 40-49, (in Japanese)

Shimizu,Y., Nakamura,S., Kuzuhara,S. and Kurata,S., "Studies of the Configuration and Performance of Annular Type Jet Pumps", Trans. ASME,J. Fluids Eng.,109,(1987),205-212

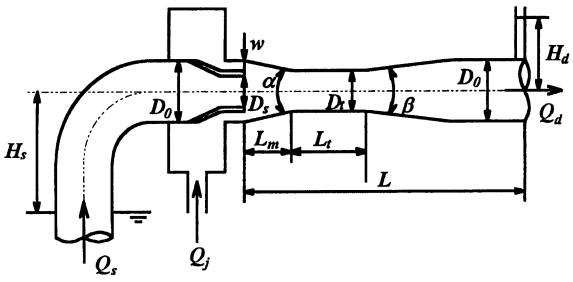

Fig.1 Schematic of annular jet pump

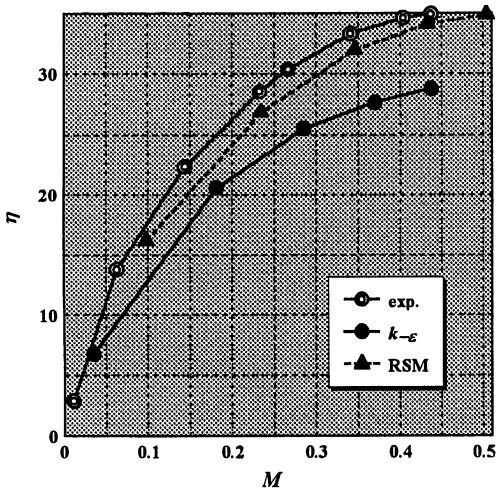

Fig.2 Comparison of predicted efficiency with two models

Table 1 Definitions and dimensions of jet pumps

Symbol	Definition	Type-1	Type-2
D_0	Inner Diameter	55.0 (mm)	55.0 (mm)
D_s	I. Dia. of Suction Pipe	43.0 (mm)	47.0 (mm)
D_t	I. Dia. of Throat	38.0 (mm)	24.3 (mm)
L_m	Length of Nozzle	31.7 (mm)	26.6 (mm)
L_t	Length of Throat	102.3 (mm)	123.3 (mm)
w	Clearance	4.0 (mm)	2.0 (mm)
α	Convergence Angle	30.0 (deg)	60.0 (deg)
β	Divergence Angle	5.8 (deg)	5.8 (deg)
H_s	Head of Suction Flow	1.00 (m)	1.00 (m)
H_d	Head of Exit Flow	1.48 (m)	1.48 (m)

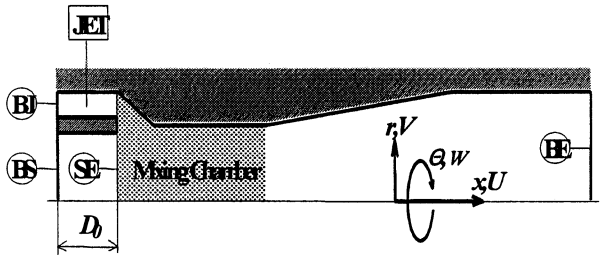

Fig.3 Computational domain and coordinate system

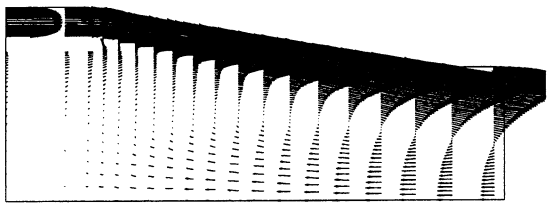

(a) Re=5.5×10^5

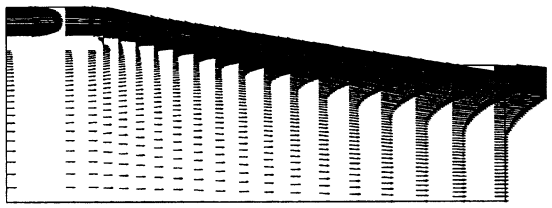

(b) Re=7.7×10^5

Fig.4 Mean velocity vectors in x-r plane (Type-1)

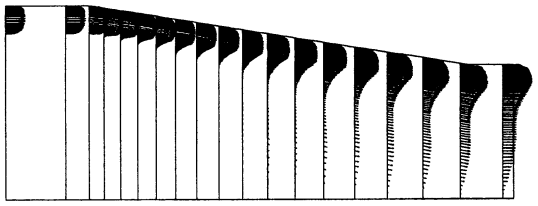

(a) Re=5.5×10^5

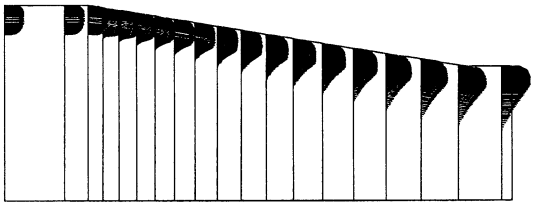

(b) Re=7.7×10^5

Fig.5 Mean velocity vectors in r- θ plane (Type-1)

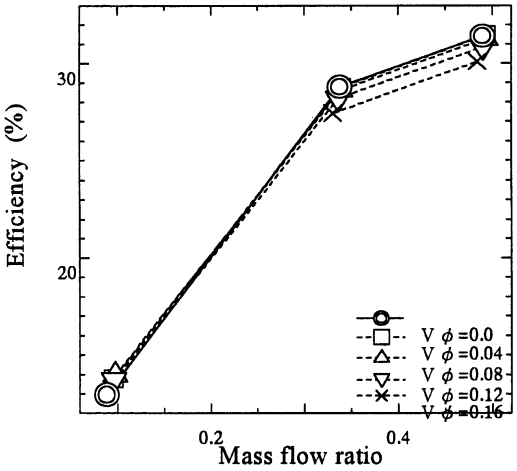

Fig.6 Predicted efficiencies at different inlet swirls (Type-1)

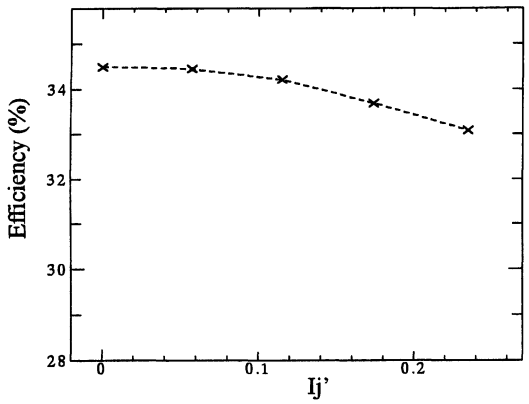

Fig.7 Predicted efficiency at Re=7.7×10^5 (Type-1)

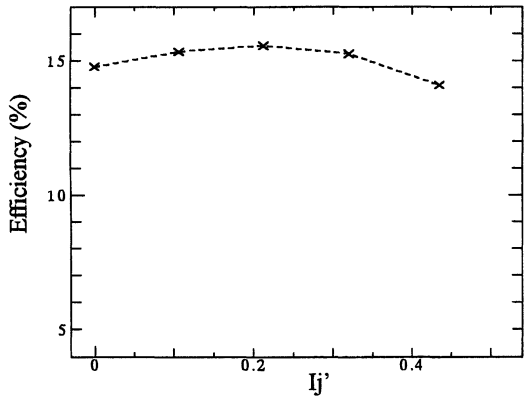

Fig.8 Predicted efficiency at Re=5.5×10^5 (Type-1)

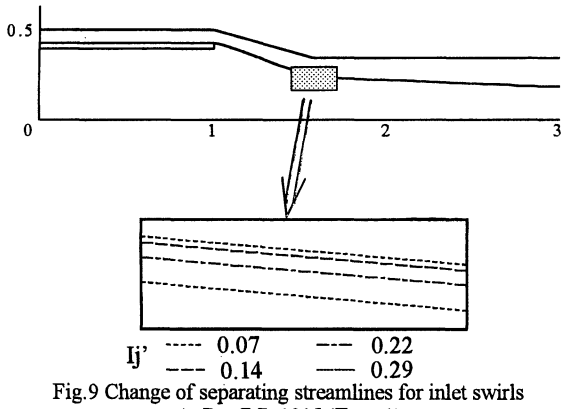

Fig.9 Change of separating streamlines for inlet swirls At Re=7.7×10^5 (Type-1)

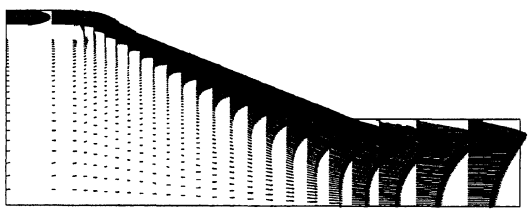

Fig.10 Mean velocity vectors in x-r plane (Type-2)

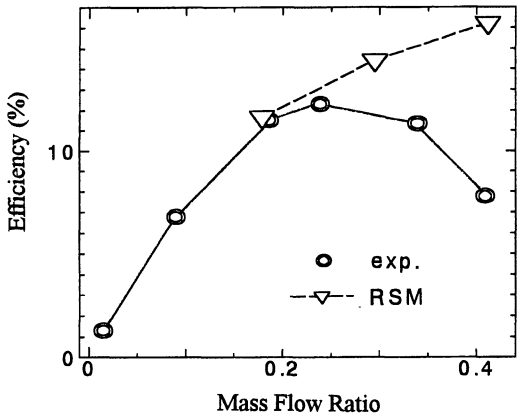

Fig.11 Comparison of predicted efficiency with experiment (Type-2)

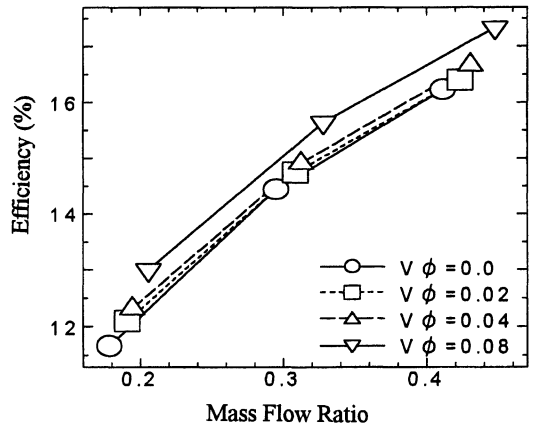

Fig.12 Calculated efficiency at various inlet swirls (Type-2)

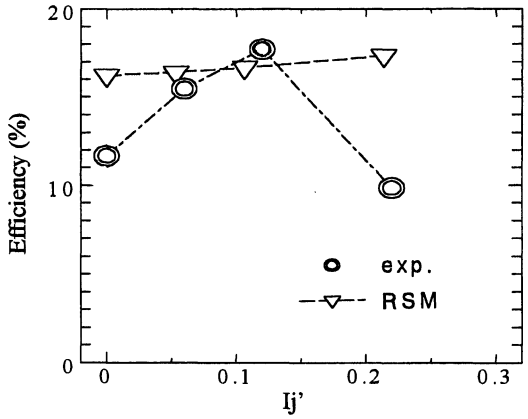

Fig.13 Comparison of predicted efficiency with experiment (Type-2)